Nano Research
2022, 15(1): 225–229
ISSN 1998-0124 CN 11-5974/O4
https://doi.org/10.1007/s12274-021-3463-3

Research Article

Graphene foam resonators: Fabrication and characterization

Yahav Ben-Shimon, Siva K. Reddy, and Assaf Ya'akobovitz (✉)

Department of Mechanical Engineering, Faculty of Engineering Sciences, Ben-Gurion University of the Negev, Israel

Received: 27 January 2021 / **Revised:** 5 March 2021 / **Accepted:** 20 March 2021

ABSTRACT

Three-dimensional graphene foams (GFs) benefit from a large surface area and unique physical properties. We present here the first-ever miniaturized GF-based resonators. We developed a simple yet reliable fabrication process, in which GFs are synthesized and assembled on a cavity to form suspended GF devices. We electrostatically excited these devices and analyzed their resonance and ring-down responses. We observed significant energy dissipation, as the quality factor of the devices was in the order of several tens. Additionally, we investigated the influence of temperature on the operation of the devices and found that high temperatures mechanically soften the resonators but also considerably enhance energy dissipation. Finally, our devices demonstrated a mode-coupling of a resonance mode and a mode having twice its frequency. Thus, this work paves the way toward the development of novel GF resonators that could be integrated into future devices, such as GF-based nano-electromechanical sensors, electrical circuits, and oscillators.

KEYWORDS

energy dissipation, graphene foam, micro/nano electromechanical systems, three-dimensional graphene, resonators

1 Introduction

A three-dimensional (3D) graphene foam (referred to here as GF) is an open-cell nano-material comprising a 3D network of hollow multilayer graphene branches. The 3D microscopic structure of the GF dictates a highly porous nanostructure and, as a result, unique physical properties that are different than those of its two-dimensional counterpart. For example, GF is mechanically compliant [1], its thermal conductance relates to its density [2], and it has a broadband energy absorption [3]. The mainstream method for the synthesis of high-quality GF is the high-temperature chemical vapor deposition (CVD) process, in which the carbon is introduced via the growth gas and graphene layers are crystalized on a metal scaffold. After growth, the metal is etched such that only the GF structure is left.

Owing to their unique properties and structure, GFs were successfully integrated into a wide range of functional systems, including electrochemical capacitors [4], strain sensors [5], wearable sensors [6], composite reinforcements [7], electromagnetic shields [8], thermal devices [9], and energy-conversion applications [3], to name but a few. Furthermore, the electromechanical behavior of rather large (centimeter-scale) GFs was recently investigated, and their ability to be electrostatically excited was demonstrated [10]. Thus, GFs hold the promising potential to be integrated as porous nano-materials into electrostatically actuated micro/nano electromechanical system (MEMS/NEMS) devices, electromechanical filters, resonating sensors, etc.

Resonators are among the most important applications for MEMS/NEMS devices. They are typically excited around one of their resonance frequencies (in most cases, around their fundamental frequency), where the response is dynamically amplified. Commonly, the resonators are excited using an electrostatic force [11], although other excitation methods were reported, such as piezoelectric [12] and magnetic excitation [13]. Micron-scale devices demonstrate excitation frequencies in the kilo-Hertz range [11]. Among the vast variety of resonators applications are mass sensors [14], clocking devices [15], accelerometers [16], logic devices [17], optical devices [18], and bandpass filters [19].

Porous electromechanical devices have been intensively studied in previous years. Due to their ultra-high surface area, they are attractive for a plethora of applications, such as humidity sensors [20], RF devices [21], gas sensors [22], biosensors [23], and optical filters [24]. However, the synthesis of a porous layer, such as porous silicon, dictates a complicated fabrication process that often involves the electrochemical etching of the device layer to create the porous structure. In the present study, we describe the fabrication and characterization of porous GF resonators that benefit from a simple fabrication process, high yield, and high-frequency operation. We thereby built, for the first time, miniaturized suspended GF resonators and studied their dynamic operation, their dissipation characteristics, and the influence of temperature on their behavior.

2 Methods

The GF resonators were grown in a high-temperature chemical vapor deposition (CVD) process. Porous (95% porosity) nickel (Sigma-Aldrich) was used as the sacrificial scaffold for the GF growth. The porous nickel was placed in a tube furnace and the temperature was ramped to 860 °C while helium (500 SCCM) and hydrogen (200 SCCM) were introduced. The temperature and gas flow rates were maintained for 40 min during the annealing of the nickel. Then, the growth started by flowing

Address correspondence to assafyaa@bgu.ac.il

20 SCCM of ethylene (C_2H_4) for 20 min, after which the ethylene flow was stopped, and the Ni-GF was cooled back to room temperature. Next, the Ni-GF was coated with a protective layer of polymethyl methacrylate (PMMA) and the nickel was wet-etched with HCl for 7 h. Finally, the PMMA was removed by dipping the GF-PMMA into acetone heated to 70 °C. The mass density of the grown GF was measured to be 1.3 ± 0.6 gr/cm^3, which is similar to values reported in the literature and comparable to the density of boron-nitride foam [25]. Notably, Young's modulus of our devices was found to be ~ 10 kPa [10].

Electrical contacts were formed by putting a thin strip of conductive silver paste that covered both part of the anchored GF (i.e., part of the GF that is attached to the wafer and are not suspended) and the wafer. To avoid direct contact with the fragile GF, we electrically interfaced the part of the silver paste that covers the wafer. Electrical measurements were obtained by forming two of those electrical contacts (one on each side of the GF) and using a precision source measurement unit (SMU, Keysight B2902A) that applied voltage along the GF resonators while measuring the induced current. In addition, a digital multimeter (DMM, Keithley 2110-240) was used to conduct capacitance measurements between the GF and the wafer.

The resonance response of the GF resonators was characterized by using a network analyzer (Keisight E5061B), that was electrically connected to the GF resonators through the silver paste. The network analyzer applied a time-dependent excitation voltage to the GF resonators, while the excitation frequency was swept. A laser Doppler vibrometer (LDV, Polytec MSA-500M) was used to capture the time response of the vibrating GF resonator and its analog output was analyzed by the network analyzer, which yielded the frequency response of the GF resonators. GF resonators that were subjected to high temperatures were similarly characterized, but they were mounted on a computer-controlled hot-plate.

3 Results and discussion

GF resonators were first micro-fabricated. Heavily doped silicon wafers covered by a thin (1 μm) layer of silicon dioxide (SiO_2) were used as a starting material, Fig. 1(a). Large cavities (4 mm squares) were created in the SiO_2 layer by lithography and HF acid wet-etch, Fig. 1(b). In parallel, the GF was CVD-grown, after which it was attached to the pre-patterned wafer such that it covered the cavities, and the GF was suspended, Fig. 1(c). Importantly, this process demonstrated a yield of 100%. Optical and scanning electron microscope (SEM) images of the GF are shown in Figs. 1(d) and 1(e), respectively. The Raman spectrum of the GF resonator is shown in Fig. 1(f), indicating the G- and 2D-bands, which are typical for graphene sheets. The ratio between the intensities of the G- and D-bands indicates that our devices comprise multilayer graphene. Additionally, the intensity of the D-band is low and is indicative of a low concentration of defects. Energy dispersive spectroscopy (EDS) measurement confirmed the existence of carbon atoms with negligible nickel residuals, Fig. 1(g). Furthermore, X-ray diffraction (XRD) patterns were acquired before and after the nickel etch process, Fig. 1(h). Before the nickel etch process, the peaks related to nickel (111), (200), and (220) planes and graphitic carbon (002) plane, were observed. However, after the nickel was etched, only the patterns related to graphitic carbon remained, indicating again the complete removal of the nickel.

Our analysis started with investigating the electrical properties of the GF resonators. Two-points current-voltage (I–V) measurements were first conducted, Fig. 2(a). The GF resonators demonstrated linear I–V characteristics, which can be attributed

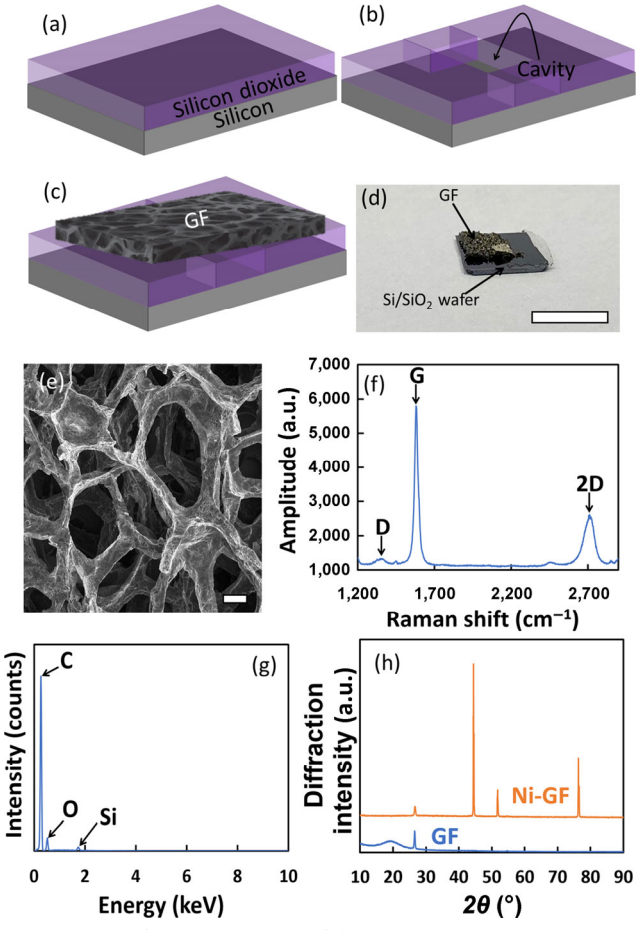

Figure 1 The fabrication process of the GF resonators. (a) The starting material is a Si/SiO_2 wafer. (b) Lithography and wet-etch (using HF acid) of the cavities. (c) Attachment of the GF to cover the cavities. (d) Optical image of a GF resonator suspended over a cavity. Scale bar: 1 cm. (e) SEM image of the GF. Scale bar: 100 μm. (f) Raman spectrum of a GF resonator, showing the D-, G- and 2D-bands. (g) EDS of GF resonator. The existence of carbon, silicon, and oxygen are indicated. (h) XRD patterns of GF and Ni-GF.

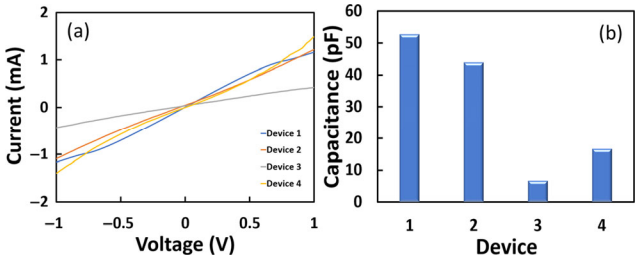

Figure 2 Electrical characteristics of GF resonators. (a) I–V curves. (b) Capacitance measurements.

to the semi-metallic energy band structure of graphene and the multilayer structure of the devices. Next, the capacitance of the GF resonators was analyzed. First, the total capacitance of the GF (which includes both the anchored and the suspended GF) with respect to the silicon wafer, was measured. Then the capacitance of the anchored GF was subtracted from the total capacitance, such that the capacitance values shown in Fig. 2(b) refer only to the suspended GF capacitance. Notably, these capacitance values are comparable to those calculated for parallel plate capacitor having the same geometry. This observation agrees with previous findings that showed that despite the porous structure of the GF and the induced electrostatic fringe field, the capacitance of GF is comparable to parallel plate capacitor with the same dimensions [10].

We first excited the devices by applying a time-dependent voltage between the silicon substrate and the suspended GF, which induced an electric field. The electric field generates a force that attracts the GF toward the substrate, while the elasticity of the GF acts as the restoring force, pulling the GF back toward its initial position. Notably, due to the porous structure of the GF, the induced electrostatic field is different than that created between flat electrodes, and it comprises mostly fringe field lines. The experimental setup, illustrated in Fig. 3(a), includes an LDV, which was used to capture the vibration of the devices, and a network analyzer, which provided the excitation voltage and analyzed the device vibrations in the frequency domain.

We began our electrostatic analysis with two types of experiments. In the first experiment, an excitation voltage in the form of $V(t) = V_{DC} + V_{AC}\sin(2\pi ft)$ (V_{DC} and V_{AC} are the bias and time-dependent voltage components, respectively, f is the excitation frequency, and t is the time) was applied to the devices and the excitation frequency was swept to obtain the frequency response of the devices. In the second experiment, the devices were subjected to a short electrical pulse of 400 V, applied for ~100 μs, allowing us to capture the decaying time response of our devices, i.e., their ring-down response.

The frequency response of a representative GF resonator (other devices demonstrated similar behavior) is shown in Fig. 3(b) and corresponds to the Lorentzian function

$$A(f) = \frac{\delta_{st}}{\sqrt{\left(1-\left(\frac{f}{f_r}\right)^2\right)^2 + \left(\frac{f}{f_r Q}\right)^2}} \quad (1)$$

where A is the vibrational amplitude, δ_{st} is the static deflection, f and f_r are the excitation and resonance frequencies, respectively, and Q is the quality factor. We extracted the resonance frequency and the quality factor by fitting the acquired frequency response to the Lorentzian function. Notably, many resonance modes arose during the excitation of the devices, most of which represent local vibration modes where only a part of the structure vibrated. However, the resonance frequency response, shown in Fig. 3(b), corresponds to the resonance vibration of the whole structure, as verified by the sampling of multiple points using the scanning mode of the LDV, which showed that the structure moved as a whole.

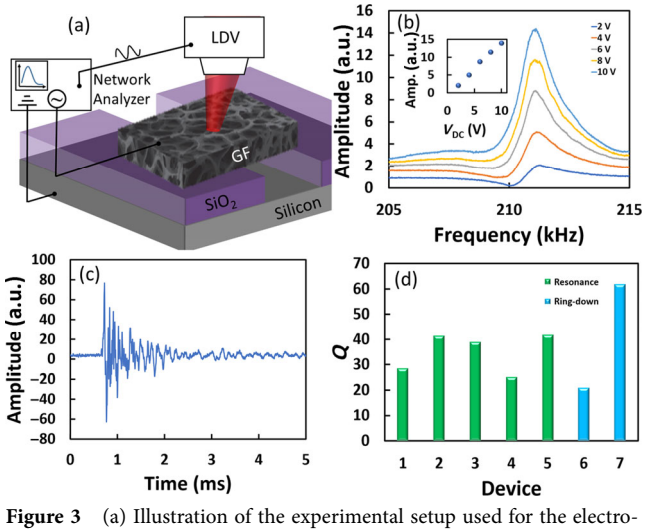

Figure 3 (a) Illustration of the experimental setup used for the electromechanical characterization of the GF resonators. (b) Frequency response of a representative GF resonator. Different colors represent different bias voltages. Inset: the relationship between the maximal vibrational amplitude and the bias component of the excitation voltage. (c) Time response of a GF resonator subjected to a short electrical pulse. (d) Quality factor extracted for seven devices investigated under resonance (green bars) and ring-down (blue bars) conditions.

The frequency response of the GF resonator shown in Fig. 3(b) demonstrated a clear resonance around 211 kHz. The relationship between the bias component of the excitation voltage and the maximum vibrational amplitude is shown as an inset in Fig. 3(b). As expected, since the excitation force is proportional to V_{DC}, the vibration amplitude is proportional to the bias component. Moreover, our devices were suspended over large cavities (4 mm squares), which are usually associated with low resonance frequencies. In addition, a previous study showed that GFs have a low stiffness when subjected to electrostatic pressure [10], which also contributes to low resonance frequency. However, due to the extremely low mass density of GF devices, they demonstrated high resonance frequencies, ranging between tens to hundreds of kilo-Hertz.

The ring-down response of a representative device is shown in Fig. 3(c). This response can be approximated by the following decaying term [26]

$$u(t) = A\exp\left(-\frac{\pi ft}{Q}\right)\sin\left(2\pi f_d t + \phi\right) \quad (2)$$

where t is time, f_d is the damped frequency of vibration, $A = \sqrt{u_0^2 + \left(\frac{v_0 + 2\pi f_n u_0 / 2Q}{2\pi f_d}\right)^2}$, and $\tan f = \frac{2\pi f_d u_0}{v_0 + 2\pi f_d u_0 / 2Q}$ (u_0 and v_0 are the initial deflection and velocity, respectively, and f_n is the natural frequency). Notably, despite the electrostatic pulse that was applied to the device, and contrary to the frequency response experiments (Fig. 3(b)), the ring-down response is mechanical by nature and is governed by the elasticity of the device and the damping. The logarithmic decay method was used to extract the quality factor from this decaying response [26]

$$Q^{-1} = \frac{1}{\pi k}\log\left(\frac{A_i}{A_{i+k}}\right) \quad (3)$$

where A_i and A_{i+k} are the k and $k+1$ peak deflection amplitudes, respectively. The quality factors of several devices subjected to either time-dependent voltage (i.e., resonance response) or a short pulse (i.e., ring-down response), shown in Fig. 3(d), demonstrate similar values, in the order of several tens. These values are considered to be somewhat low, however, they are comparable to values reported in other studies, in which two-dimensional materials were excited in ambient conditions [27].

The quality factor represents the relationship between the steady-state oscillation energy, E_{SS}, and the dissipated energy per cycle, E_{loss}, namely

$$Q = 2\pi\frac{E_{SS}}{E_{loss}} \quad (4)$$

Thus, the low quality factor values indicate a significant energy dissipation. Many dissipation mechanisms have been identified in miniaturized electromechanical devices—including air dissipation, thermoelastic losses [28, 29], surface losses [30], clamping losses [31], and more—which also influenced our GF resonators. Due to the porous structure of the devices, we attribute most of the dissipation to air losses and surface losses, which are both related to the large surface area. Air dissipation and, more importantly, squeeze-film air damping exists in our experiment, as air molecules that are trapped in the cavity (namely, under the suspended GF) are squeezed during the vibration of the device. The GF has an open cell structure that

enables air molecules to flow through it, but a previous study showed that, despite this perforated structure, the flow of air molecules is relatively slow, such that the trapped air is squeezed. Other studies showed that surface losses, which are assciated to defects related to the atomic lattice at the surface and to surface contaminations, are more pronounced in devices with high surface-to-volume ratios. As GF devices have an extremely high surface-to-volume ratio, surface losses are also dominant. In addition, previous observations indicated that electrostatic forces generate relative motion between the graphene layers – a sliding motion that also enhances the material dissipation of the GF. Taken together, the combination of dominant squeeze-film air dissipation, surface losses, and material losses results in significant energy dissipation, which manifests in the low-quality factor values, shown in Fig. 3(d).

Next, we investigated the dynamic response of several GF resonators under various temperatures. To this end, the devices were excited around their resonance while mounted on a hot-plate, which applied temperatures between room temperature and 100 °C, Fig. 4(a). Increasing the temperature has two main effects on the dynamic response of the resonators: both the resonance frequency and the quality factor decreased when the temperature was increased, Figs. 4(b) and 4(c). The decrease in resonance frequency is attributed to the softening effect of high temperatures. Figure 4(b) shows that the resonance frequencies of GF resonators moderately decreased when the temperature is increased, indicating that the softening has a minor influence on the dynamics of the GF resonators. On the other hand, the low quality factor values imply that the high temperature enhanced energy dissipation. Indeed, the high temperature increases thermoelastic damping, which is proportional to the applied temperature [32]. Additionally, the high temperature enhances air dissipation, as it increases the kinetic energy of the surrounding air molecules, which, in turn, increases their probability of colliding with the GF. Multiple collisions between air molecules and the GF increase the thermomechanical coupling between the GF and the air molecules and, therefore, increase the dissipation of energy. While the softening contributes to larger vibration amplitudes, the lower quality factor has the opposite effect of reducing the amplitude. Our observation shows that the influence of the quality factor is more pronounced, as high temperatures are associated with lower amplitudes, Fig. 4(d).

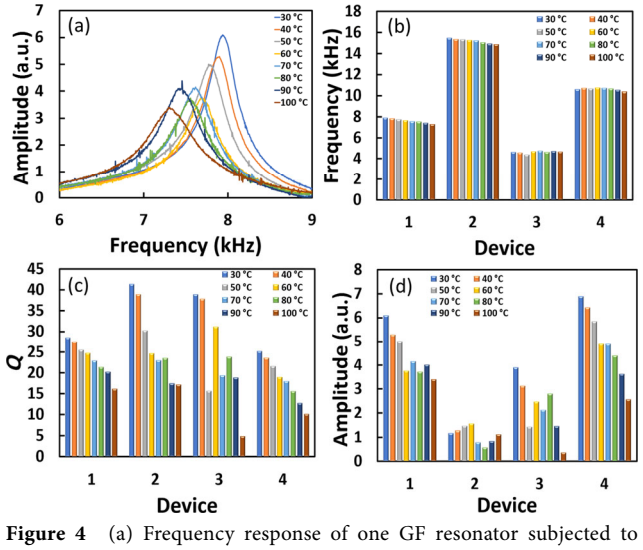

Figure 4 (a) Frequency response of one GF resonator subjected to high temperature, and the (b) resonance frequency, (c) quality factor, and (d) vibrational amplitude of several devices subjected to high temperatures.

Finally, some of our devices showed mode coupling between their resonance mode and an additional mode with twice its resonance frequency (1:2 ratio). These devices were excited at their resonance frequencies and a fast Fourier transform (FFT) applied to their time response revealed responses at the excitation frequency and twice the excitation frequency, Fig. 5(a). Increasing the excitation voltage led to a moderate increase of the vibrational amplitude associated with the excitation resonance, while the vibrational amplitude associated with the higher frequency demonstrated a much more significant increase, Fig. 5(b). This observation reveals the mode–coupling between these modes, where energy is transferred from the resonance mode to the higher mode.

The resonators characterized in this work were synthesized under the same conditions. However, they differ from one another due to variance in their morphology. For example, they have different directions and sizes of their pores and different numbers of layers. In addition, the GF resonators show variance in atomic-scale defects, such as grain boundaries, impurities, lattice imperfections, internal stress, etc. As a result, different GF resonators showed different values of resonance frequencies and quality factors. This was also reflected in previous studies where the mechanical properties of GF devices scattered over a wide range [10]. Notably, other nano-materials showed a similar distribution of their physical properties. For instance, carbon nanotube forests synthesized under the same conditions demonstrated a wide range of heat transfer characteristics [33], and GaTe devices from the same solid-crystal source exhibited large distribution of their Young's modulus [34]. Nevertheless, all of our GF resonators presented similar qualitative behavior. The GF resonators show operational frequencies in the kilo-Hertz range, which is comparable to the resonance frequencies of most MEMS devices. However, the fabrication process of the GF resonators is significantly simpler than that of MEMS devices, as high-resolution lithography or etching are not required. In addition, the significant dissipation of the GF resonators dictates a wide bandwidth, which is desired for many applications, such as communication systems and inertial sensors. Finally, the porous structure of the GF resonators is attractive for chemical sensors and electrochemical capacitors thanks to their large surface area.

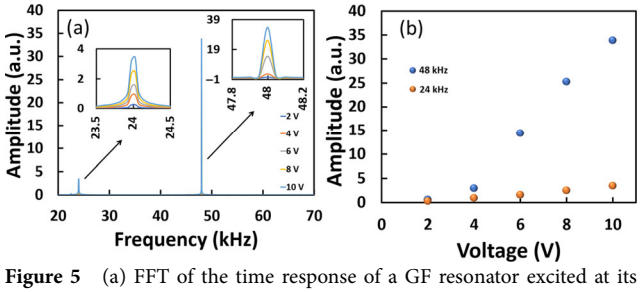

Figure 5 (a) FFT of the time response of a GF resonator excited at its resonance frequency (24 kHz). (b) Vibrational amplitude versus the bias component of the voltage.

4 Conclusion

We developed a simple and reliable fabrication process of GF resonators. The devices were electrostatically excited around their resonance frequencies and demonstrated significant energy dissipation due to squeeze-film air damping, surface losses, and material damping. Exciting the devices under high temperatures mechanically softened the GF resonators and further enhanced energy dissipation. A 1:2 ratio mode-coupling was manifested by energy transfer from the lower frequency mode to the higher frequency mode. Such mode-coupling is highly attractive for a

wide range of applications, where energy needs to be transferred between different modes (e.g., in rate sensors) or where the vibration amplitude and frequency need to be carefully controlled (e.g., in clocking devices). The porous structure of the GF resonators and their high surface area open the path for the development of novel porous resonators that are desired for chemical and biological sensors.

References

[1] Reddy, S. K.; Ferry, D. B.; Misra, A. Highly compressible behavior of polymer mediated three-dimensional network of graphene foam. *RSC Adv*. **2014**, *4*, 50074–50080.

[2] Pettes, M. T.; Ji, H. X.; Ruoff, R. S.; Shi, L. Thermal transport in three-dimensional foam architectures of few-layer graphene and ultrathin graphite. *Nano Lett*. **2012**, *12*, 2959–2964.

[3] Ren, H. Y.; Tang, M.; Guan, B. L.; Wang, K. X.; Yang, J. W.; Wang, F. F.; Wang, M. Z.; Shan, J. Y.; Chen, Z. L.; Wei, D. et al. Hierarchical graphene foam for efficient omnidirectional solar–thermal energy conversion. *Adv*. *Mater*. **2017**, *29*, 1702590.

[4] Brownson, D. A. C.; Figueiredo-Filho, L. C. S.; Ji, X. B.; Gómez-Mingot, M.; Iniesta, J.; Fatibello-Filho, O.; Kampouris, D. K.; Banks, C. E. Freestanding three-dimensional graphene foam gives rise to beneficial electrochemical signatures within non-aqueous media. *J. Mater*. *Chem*. *A* **2013**, *1*, 5962–5972.

[5] Samad, Y. A.; Li, Y. Q.; Alhassan, S. M.; Liao, K. Novel graphene foam composite with adjustable sensitivity for sensor applications. *ACS Appl*. *Mater*. *Interfaces* **2015**, *7*, 9195–9202.

[6] Xu, R.; Zhang, H.; Cai, Y.; Ruan, J.; Qu, K.; Liu, E.; Ni, X.;. Lu, M.; Dong, X. ,Flexible and wearable 3D graphene sensor with 141 KHz frequency signal response capability. *Appl*. *Phys*. *Lett*. **2017**, *111*, 103501.

[7] Xu, R. Q.; Lu, Y. Q.; Jiang, C. H.; Chen, J.; Mao, P.; Gao, G. H.; Zhang, L. B.; Shan, W. Facile fabrication of three-dimensional graphene foam/poly (dimethylsiloxane) composites and their potential application as strain sensor. *ACS Appl*. *Mater*. *Interfaces* **2014**, *6*, 13455–13460.

[8] Chen, Z. P.; Xu, C.; Ma, C. Q.; Ren, W. C.; Cheng, H. M. Lightweight and flexible graphene foam composites for high-performance electromagnetic interference shielding. *Adv*. *Mater*. **2013**, *25*, 1296–1300.

[9] Cohen, Y.; Reddy, S. K.; Ya'akobovitz, A. Heat dissipation in graphene foams. *Nano Res*. **2021**, *14*, 829–833.

[10] Reddy, S. K.; Ya'akobovitz, A. Electromechanical behavior of graphene foams. *Appl*. *Phys*. *Lett*. **2019**, *115*, 211902.

[11] Ya'akobovitz, A.; Krylov, S. The influence of perforation on electrostatic and damping forces in thick SOI MEMS structures. *J. Micromech*. *Microeng*. **2012**, *22*, 115006.

[12] Kon, S.; Horowitz, R. A high-resolution MEMS piezoelectric strain sensor for structural vibration detection. *IEEE Sens*. *J*. **2008**, *8*, 2027–2035.

[13] Ben-Shimon, Y.; Ya'akobovitz, A. Magnetic excitation and dissipation of multilayer two-dimensional resonators. *Appl*. *Phys*. *Lett*. **2021**, *118*, 063103.

[14] Li, M.; Tang, H. X.; Roukes, M. L. Ultra-sensitive NEMS-based cantilevers for sensing, scanned probe and very high-frequency applications. *Nat*. *Nanotechnol*. **2007**, *2*, 114–120.

[15] van Beek, J. T. M.; Puers, R. A review of MEMS oscillators for frequency reference and timing applications. *J. Micromech*. *Microeng*. **2011**, *22*, 013001.

[16] Halevy, O.; Krakover, N.; Krylov, S. Feasibility study of a resonant accelerometer with bistable electrostatically actuated cantilever as a sensing element. *Int*. *J*. *Non*.*-Linear*. *Mech*. **2020**, *118*, 103255.

[17] Ilyas, S.; Younis, M. I. Resonator-based M/NEMS logic devices: Review of recent advances. *Sens*. *Actuators A*: *Phys*. **2020**, *302*, 111821.

[18] Ya'akobovitz, A.; Krylov, S.; Shacham-Diamand, Y. Large angle SOI tilting actuator with integrated motion transformer and amplifier. *Sens*. *Actuators A*: *Phys*. **2008**, *148*, 422–436.

[19] Hafiz, M. A. A.; Kosuru, L.; Hajjaj, A. Z.; Younis, M. I. Highly tunable narrow bandpass MEMS filter. *IEEE Trans*. *Electron Devices* **2017**, *64*, 3392–3398.

[20] Kim, S. J.; Park, J. Y.; Lee, S. H.; Yi, S. H. Humidity sensors using porous silicon layer with mesa structure. *J*. .*Phys*. *D*: *Appl*. *Phys*. **2000**, *33*, 1781–1784.

[21] Ding, Y.; Liu, Z.; Liu, L.; Li, Z. A surface micromachining process for suspended RF-MEMS applications using porous silicon. *Microsyst*. *Technol*. **2003**, *9*, 470–473.

[22] Seals, L.; Gole, J. L.; Tse, L. A.; Hesketh, P. J. Rapid, reversible, sensitive porous silicon gas sensor. *J*. *Appl*. *Phys*. **2002**, *91*, 2519–2523.

[23] Shtenberg, G.; Massad-Ivanir, N.; Fruk, L.; Segal, E. Nanostructured porous Si optical biosensors: Effect of thermal oxidation on their performance and properties. *ACS Appl*. *Mater*. *Interfaces* **2014**, *6*, 16049–16055.

[24] Lammel, G.; Schweizer, S.; Schiesser, S.; Renaud, P. Tunable optical filter of porous silicon as key component for a MEMS spectrometer. *J*. *Microelectromech*. *Syst*. **2002**, *11*, 815–827.

[25] Xue, Y., M.; Dai, P. C.; Zhou, M.; Wang, X.; Pakdel, A.; Zhang, Q. H.; Takei, T.; Fu, X. W.; Popov, Z. I. et al. Multifunctional superelastic foam-like boron nitride nanotubular cellular-network architectures. *ACS Nano*, **2017**, *11*, 558–568.

[26] Meirovitch, L. *Elements of Vibration Analysis*; 2nd ed. McGraw-Hill: New York, 1986.

[27] Hu, K., M.; Bo, P.; Li, X. Y.; Xin, Y. H.; Bai, X. R.; Li, L.; Zhang, W. M. Resonant nano-electromechanical systems from 2D materials. *EPL*. **2020**, *131*, 58001.

[28] Lifshitz, R.; Roukes, M. L. Thermoelastic damping in micro- and nanomechanical systems. *Phys*. *Rev*. *B* **2008**, *61*, 5600–5609.

[29] Srikar, V. T.; Senturia, S. D. Thermoelastic damping in fine-grained polysilicon flexural beam resonators. *J*. *Microelectromech*. *Syst*. **2002**, *11*, 499–504.

[30] Yasumura, K. Y.; Stowe, T. D.; Chow, E. M.; Pfafman, T.; Kenny, T. W.; Stipe, B. C.; Rugar, D. Quality factors in micron- and submicron-thick cantilevers. *J*. *Microelectromech*. *Syst*. **2000**, *9*, 117–125.

[31] Ko, J. H.; Jeong, J.; Choi, J.; Cho, M. Quality factor in clamping loss of nanocantilever resonators. *Appl*. *Phys*. *Lett*. **2011**, *98*, 171909.

[32] Duwel, A.; Gorman, J.; Weinstein, M.; Borenstein, J.; Ward, P. Experimental study of thermoelastic damping in MEMS gyros. *Sens*. *Actuators A*: *Phys*. **2003**, *103*, 70–75.

[33] Cohen, Y.; Reddy, S. K.; Ben-shimon, Y.; Ya'akobovitz, A. Height and morphology dependent heat dissipation of vertically aligned carbon nanotubes. *Nanotechnology* **2019**, *30*, 505705.

[34] Chitara, B.; Ya'akobovitz, A. High-frequency electromechanical resonators based on thin GaTe. *Nanotechnology* **2017**, *28*, 42LT02.